Research Article

Thomas A. Grant*, Anton N. Vetlugin, Eric Plum, Kevin F. MacDonald* and Nikolay I. Zheludev

Localization of nanoscale objects with light singularities

Abstract: Unprecedented atomic-scale measurement resolution has recently been demonstrated in single-shot optical localization metrology based on deep-learning analyses of diffraction patterns of topologically structured light scattered from objects. Here we show that variations in the diffraction patterns caused by positional changes of an object depend upon the spatial derivatives of the magnitude and phase of the incident field, with the latter strongly enhanced around phase singularities. Despite lower intensity near the singularity, an orders-of-magnitude increase in Fisher information contained in the diffraction patterns can be achieved when a nano-object is illuminated by light containing phase singularities, rather than a plane wave. Our work provides a fundamental explanation and motivation for singularity-based metrology with deeply subwavelength precision.

Keywords: superoscillation; singularities; nanophotonics.

1 Introduction

In recent decades, progress in optical super-resolution microscopy and metrology has been driven by nonlinear and statistical techniques [1-11], structured illumination microscopy [12-14], and computational imaging techniques for retrieving phase from scattered light [15-21], often taking advantage of object sparsity [22-24]. The ability of neural networks to efficiently solve the inverse scattering problem has also been demonstrated [25], and superoscillatory (topologically structured) light fields have lately been applied to microscopy and optical metrological applications in a manner similar to computational imaging.

The phenomenon of optical superoscillation was first introduced [26] in 2006 and experimentally identified shortly thereafter [27]. It describes rapid subwavelength spatial variations of intensity and phase in complex electromagnetic fields formed by the interference of several coherent waves, and its discovery stimulated a significant revision of the limits of classical electromagnetism. In particular, the computational and experimental studies of the topological structure of superoscillatory fields in free space revealed arbitrarily small energy 'hotspots' and high local wavevectors, facilitated by the presence of phase singularities bordering regions of energy backflow (i.e. powerflow vortices) [28,29]. These can be orders of magnitude smaller than the wavelength, implying that their interaction with matter should vary on similarly short, subwavelength scales making their application an intriguing prospect for metrology.

Berry and Nye proposed a form of singularity-based metrology in the 1970s, suggesting that singularities (referred to then as 'wave dislocations') in radio pulses reflected by the rock bed of a glacier could be employed as subwavelength markers for echosounding-based depth measurements [30,31]. More recently, dimensional and positional measurements with deeply subwavelength resolution have been achieved via deep learning analysis of objects' diffraction patterns [32-34]. With topologically structured illumination and 'in-situ' neural network training, such measurements can localize the average position of a nanowire with precision and accuracy down to ~100 pm using visible light [35-36], beating the diffraction limit of conventional optical instruments thousands of times over.

In this work, we mathematically describe and numerically demonstrate that the scattering from an object located near a singularity in a topologically structured field has higher information content than the scattered field from a plane wave, thereby enabling greater precision in measurements based upon its analysis (the limit of precision being inversely proportional to Fisher information). We show analytically that this advantage derives from the presence of high phase gradients over short length scales in the incident field (i.e. in the vicinity of singularities), and demonstrate the principle computationally for an archetypal single-slit diffraction configuration, whereby Fisher information in a scattered superoscillatory field is enhanced by ~250× (compared to a plane wave incident field) when a singularity is located within the slit.

2 Theoretical Analysis

We begin with the Rayleigh-Sommerfeld model of diffraction - a mathematical manifestation of the Huygens-Fresnel principle [37]. For simplicity in the present case, we reduce this to a two-dimensional form, whereby the scattered field is expressed as a superposition of diverging circular waves radiating from a 1D array of points describing the scattering object (along x at z=0),

$$U(x) \propto i \int \widetilde{U}(x') \frac{\exp(i2\pi r/\lambda)}{r} \cos\theta \, dx'$$

where $\widetilde{U}(x')$ and U(x) denote the complex field of a monochromatic wave, with wavelength λ , at the object and the detector respectively; which are separated by a distance h in the propagation direction z, whereby $r=\sqrt{(x-x')^2+h^2}$, and $\theta=\arctan\left(\frac{x-x'}{h}\right)$.

As an archetypal scattering object, we consider a narrow slit in an otherwise opaque screen, with edges located at $x'=a\pm\delta$ (i.e. a slit of width 2δ centred at x'=a). We assume that a complex field, $\bar{U}(x')=A(x')e^{i\phi(xr)}$, is normally incident on the screen and is transmitted only through the slit. Following an

*Corresponding authors: Thomas A. Grant, Optoelectronics Research Centre, University of Southampton, SO17 1BJ, UK.

E-mail: t.a.grant@soton.ac.uk. https://orcid.org/0009-0001-0918-4614

and Kevin F. MacDonald Optoelectronics Research Centre, University of Southampton, SO17 1BJ, UK. E-mail: kfm@orc.soton.ac.uk. https://or-cid.org/0000-0003-3300-7519

Anton N. Vetlugin Centre for Disruptive Photonic Technologies, SPMS & TPI, Nanyang Technological University, Singapore, 637371, Singapore. https://orcid.org/0000-0002-2480-0462

Eric Plum Optoelectronics Research Centre, University of Southampton, SO17 1BJ, UK. https://orcid.org/0000-0002-1552-1840

Nikolay I. Zheludev Optoelectronics Research Centre, University of Southampton, SO17 1BJ, UK. Centre for Disruptive Photonic Technologies, SPMS & TPI, Nanyang Technological University, Singapore, 637371, Singapore. Hagler Institute for Advanced Study, Texas A&M University, College Station, Texas, 77843, USA. https://orcid.org/0000-0002-1013-6636.

integration by parts, we can write the scattered field, U(x) at the detector as a sum of three contributions:

$$U(x) = U_1(x) + U_2(x) + U_3(x)$$

where

$$\begin{split} U_1(x) &= A(a+\delta)e^{i\phi(a+\delta)}\,\xi(x,a+\delta)\\ &- A(a-\delta)e^{i\phi(a-\delta)}\,\xi(x,a-\delta) \end{split}$$

$$U_2(x) &= -\int\limits_{a-\delta}^{a+\delta}\frac{dA(x')}{dx'}\,e^{i\phi(x')}\xi(x,x')dx'$$

$$U_3(x) &= -i\int\limits_{a-\delta}^{a+\delta}\frac{d\phi(x')}{dx'}A(x')\,e^{i\phi(x')}\xi(x,x')dx' \end{split}$$

and

$$\xi(x, x') \propto i \int \frac{\exp(i2\pi r/\lambda)}{r} \cos\theta \ dx'.$$

Here, U_1 is the only term present in the diffracted field from an incident plane wave, while U_2 and U_3 are respectively dependent on variations in the amplitude and phase of the incident field over the scattering object. The changes in these additional contributions to the scattered field for a structured incident field, arising from changes in the object plane, can become significant in comparison to the associated change in U_1 . Thus, the spatially fast-changing features of a structured incident field can cause changes in U_2 and U_3 to dominate the total change in the scattered field.

3 Numerical Methods

As a practically relevant example, following the methods described in Refs [38-40] and recent experimental work [32,35,36], we consider a superoscillatory field formed by the linear combination of two band-limited, prolate spheroidal wave functions (PSWFs): $\tilde{U}(x') = [21.65S_2(x') + S_3(x')]W$, with W = 0.00021. While the two individual PSWFs are band-limited to $|k_0| = \omega/c$, $\tilde{U}(x')$ has a central peak focused beyond this limit

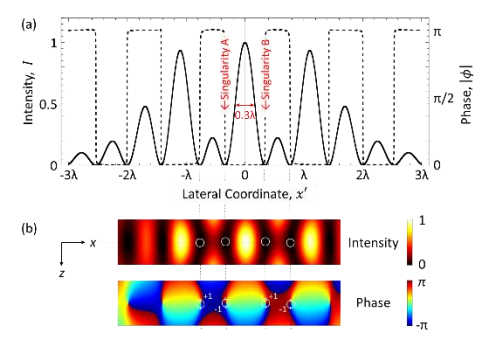


Fig. 1: Superoscillatory field profile. Intensity $I(x') = \tilde{U}(x')\tilde{U}(x')^*$ [solid line], and corresponding phase $\phi(x')$ [dashed line] profiles, of the superoscillatory field $\tilde{U}(x') = [21.65S_2(x') + S_3(x')]W$ in the object plane (z = 0). (b) Maps of intensity and phase in the xz plane – phase singularities, at low intensity points in the former, are labelled with their topological charge values in the latter.

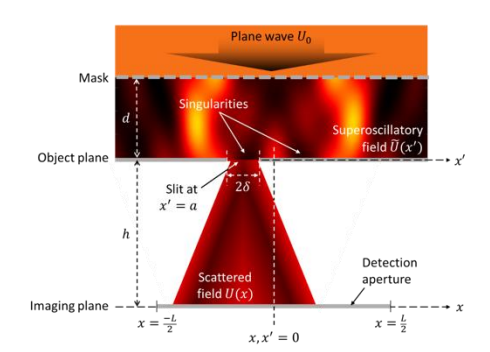


Fig. 2: Scattering of a topologically structured field by a slit in an opaque screen. A plane wave U_0 is incident upon a phase and amplitude mask, which generates a superoscillatory field $\tilde{U}(x')$ in the object plane x', with a central hotspot located at x'=0. A slit of width 2δ is centred at x'=a in the object plane. The scattered intensity $I(x)=U(x)U(x)^*$ is measured in the imaging plane x, at a distance $h=4\lambda$ beyond the object plane, with the imaging plane section (-L)/2 < x < L/2 being projected onto a detector.

(to a full-width at half-maximum of 0.3λ), flanked by a series of singularities (Fig. 1) where the phase changes abruptly but continuously over a distance $\sim \lambda/20$.

As detailed in Ref. [41], the phase and amplitude mask required to generate this superoscillatory field from a plane wave can be obtained by transforming the required object-plane field $\tilde{U}(x')$ into a Fourier series (PSWFs being eigenfunctions of a finite, band-limited Fourier transform); backpropagating to the desired mask plane; and then executing an inverse Fourier transform. Here, we assume a mask plane at a distance $d=30\lambda$ from the object plane, under which condition the intensity at the peak of the superoscillatory field's central hotspot $U(x')U(x')^*$ is approximately twice (2.06x) the intensity of the plane wave incident upon the mask, $U_0U_0^*$.

As a target object, we consider a slit of width $2\delta=\lambda/10$ in an opaque film (Fig. 2). We assume that measurements are performed by analysing its scattering pattern in an imaging plane located at a distance $h=4\lambda$ from the slit. From a practical perspective, the image sensor (detector) does not have to be at the imaging plane: the scattered field at this point is formed of free-space propagating waves, so it can be transformed to the detector plane by a conventional lens at any magnification, without loss of resolution (as has been shown experimentally [35,42]). In what follows, we assume an imaging plane detection aperture at $-\frac{L}{2} < x < \frac{L}{2\gamma}$ where $L=12\lambda$ (i.e. $\gg \delta$, a).

4 Fisher information analysis

To quantify and compare the effectiveness of localization metrology with different incident fields, we adopt the Fisher information metric, which quantifies the amount of the information that an observable variable carries about an unknown parameter upon which the probability of the observable depends [43]: A measurement that is well localized and which changes significantly in response to small changes in the unknown parameter, provides a high amount of information about that parameter. Fisher information links to achievable measurement precision through the Cramér-Rao lower bound –

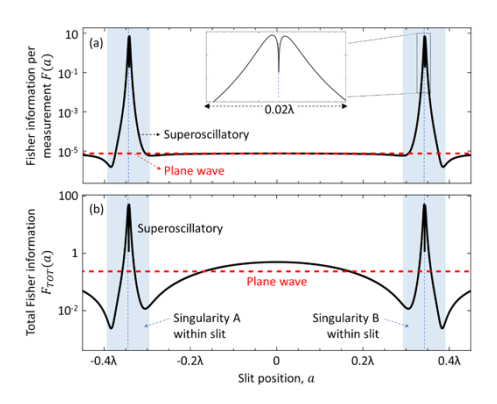


Fig. 3: Fisher information content of the field scattered by a subwavelength slit. (a) Fisher information per measurement and (b) total Fisher information as functions of slit position for: a superoscillatory incident field with amplitude [21.65 $S_2(x') + S_3(x')]W$ – shown as solid black lines; a plane wave incident field with an intensity equal to half that of the superoscillatory hotspot – shown as dashed red lines. The blue haded bands denote the range of positions over which a singularity (A or B, as labelled in Fig. 1) is located within the slit.

the reciprocal of Fisher information is a lower bound on the variance of the unknown parameter. For example, in microscopic methods based upon localization of fluorescent molecules, Fisher information is related to the point-spread-functions obtained during measurements and can be used as a tool for their optimization [44, 45]. In quantum metrology, Fisher information can be used to derive the fundamental limits applicable to parameter retrieval problems such as resolving incoherent point sources [46], time-varying waveform estimation [47], and quantum imaging [48], among others [49]. More recently, the Fisher information in classical optical scattering problems has been studied [50,51], and proposed as an optimization tool for scattering-based parameter estimation problems [52-54].

In the present case, we calculate the Fisher information by taking the scattered field – specifically the normalized distribution of the detected power (as a function of position x on the detector) at the image plane, for a given slit position, α – as a photodetection probability distribution function:

$$p(x;a) = \frac{U(x,a)U(x,a)^*}{\int_{-L/2}^{+L/2} U(x,a)U(x,a)^* dx}$$

From a measurement perspective, this density function and the relative rate of change in its log-likelihood function are important: The latter is known as the score function, and its weighted square, integrated over the detection range L, is the Fisher information, a figure of merit in the present case for how rapidly the profile of the scattered field changes in response to a change in the position α of the slit:

$$F(a) = \int_{-\frac{L}{a}}^{+\frac{L}{2}} \left[\frac{\partial}{\partial a} \ln p(x; a) \right]^{2} p(x; a) dx$$

This amounts to the information per photodetection; the total Fisher information content within the scattered field is obtained by scaling for the total power detected:

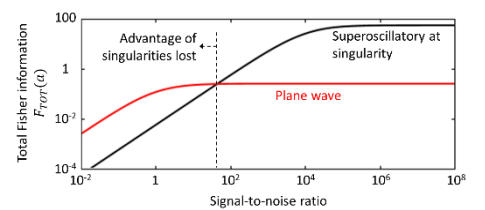


Fig. 4: Total Fisher information as a function of signal-to-noise ratio for a superoscillatory incident field (assuming the scattering to be optimally located at a singularity) [red line] and for a plane wave [blue line].

$$F_{TOT}(a) \sim F(a) \int_{-\frac{L}{2}}^{+\frac{L}{2}} U(x,a) U(x,a)^* dx$$

Figure 3 shows that the Fisher information content of a scattered superoscillatory field depends strongly on the position of the scattering object within the incident field - in this case, most prominently on the position of the slit relative to the phase singularities (as opposed to the central intensity hotspot). Note that there is no dependence of Fisher information on slit position for an incident plane wave, because while the position of the diffraction pattern in the imaging plane shifts with the slit position in the object plane, its intensity profile is invariant. For the superoscillatory field, the Fisher information increases sharply, peaking at $a = \pm 0.34\lambda$, when either singularity A or B (on either side of the incident field's central hotspot - see Fig. 1) is near the center of the slit. The double- or split-peak structure, shown in the Fig. 3a inset, is the result of a saddle point in the profile of the scattered field when the slit is perfectly centered on the singularity, whereby the scattered field is slightly less sensitive to changes in slit position than for off-center alignments. At the maxima, the intensity profile of the diffraction pattern changes rapidly as a function of a, yielding a 10^6 -fold enhancement in Fisher information (Fig. 3a), as compared to the plane wave from which the superoscillatory field was generated. The fact that incident (and therefore scattered) intensity is exponentially lower in the vicinity of phase singularities, relative to the case of a plane wave, must be considered in this comparison: Fig. 3b demonstrates that using a topologically structured incident field - i.e. probing the target object with an incident field containing singularities - nonetheless provides significant advantage, with the total information content in the detected scattered field being enhanced by a factor of ~250, again as compared to the plane wave from which the superoscillatory field was generated.

It is also important to account for the fact that measurements at low intensities near a singularity are more susceptible to noise. Within the framework of Fisher information, this can be considered as follows: Each scattered field measurement (photodetection event) provides information F(a), while (detector) noise-related photodetection events provide zero information. Fisher information is additive, so the reduction of information due to the presence of noise is proportional simply to the ratio of scattered field to noise detection events. Thus, in terms of intensity:

$$F(a, I_{noise}) = \int_{\frac{L}{2}}^{\frac{L}{2}} \left[\frac{d}{da} \ln(p(x; a)) \right]^{2} p(x; a) \frac{I(x; a)}{I(x; a) + I_{noise}} dx$$

Figure 4 shows total Fisher information as a function of signal-tonoise ratio (SNR). For consistent comparison, we assume the same plane wave intensity as used for generation of the superoscillatory field, and the same level of absolute noise in both cases. At high SNR (>1000), the advantage of the superoscillatory incident field is obvious: Fisher information is orders of magnitude higher than for a plane wave. With decreasing SNR, the information content of the scattered field falls faster for the superoscillatory field, and its metrological advantage disappears at signal to noise ratios <50.

5 Conclusion

In summary, this study provides a fundamental explanation, and justification, for singularity-based metrology. We demonstrate that when probing a nanoscale object, a significant advantage can be gained from exploiting phase singularities in a topologically structured incident field, as compared to plane wave illumination. Despite the low intensity in the vicinity of singularities, and in the presence of detector noise, the Fisher information content of a nano-object's scattering pattern can be orders of magnitude larger when it is illuminated with a topologically structured field with phase singularities, as opposed to a plane wave. We show analytically that this advantage - seen experimentally in the form of enhanced measurement precision and accuracy [35-36] - is derived from the strong dependence of scattered intensity profile on local intensity and phase gradients in the incident field at the object plane: small, deeply subwavelength changes in the position of a scattering object relative to a singularity, can lead to large changes in the scattered field. The method presented here provides a framework for optimization of the incident intensity and phase profile and object-to-imaging plane distance depending on the shape class and size range of objects.

Research funding: This work was supported by the Engineering and Physical Sciences Research Council, UK (grant number Ep/T02643X/1), and the National Research Foundation, Singapore (NRF-CRP23-2019-0006).

Author contribution: All authors have accepted responsibility for the entire content of this manuscript and approved its submission

Conflict of interest: Authors state no conflict of interest.

Data availability: Data sharing does not apply to this article as no datasets were generated or analyzed during the current study.

References

- [1] S. W. Hell and J. Wichmann, "Breaking the diffraction resolution limit by stimulated emission: stimulated-emission-depletion fluorescence microscopy," *Opt. Lett.*, vol. 19, no. 11, pp. 780-782, 1994, doi: 10.1364/0L.19.000780.
- [2] T. A. Klar and S. W. Hell, "Subdiffraction resolution in far-field fluorescence microscopy," Opt. Lett., vol. 24, no. 14, pp. 954-956, 1999, doi: 10.1364/OL.24.000954.
- [3] G. Vicidomini, P. Bianchini, and A. Diaspro, "STED super-resolved microscopy," Nat. Methods, vol. 15, no. 3, pp. 173-182, 2018, doi: 10.1038/nmeth.4593.
- [4] E. Betzig et al., "Imaging Intracellular Fluorescent Proteins at Nanometer Resolution," *Science*, vol. 313, no. 5793, pp. 1642-1645, 2006, doi: 10.1126/science.1127344.
- [5] R. Henriques, C. Griffiths, E. Hesper Rego, and M. M. Mhlanga, "PALM and STORM: Unlocking live-cell super-resolution," *Bi-opolymers*, vol. 95, no. 5, pp. 322-331, 2011, doi: 10.1002/bip.21586.

- [6] M. J. Rust, M. Bates, and X. Zhuang, "Sub-diffraction-limit imaging by stochastic optical reconstruction microscopy (STORM)," *Nat. Methods*, vol. 3, no. 10, pp. 793-796, 2006, doi: 10.1038/nmeth929
- [7] F. Balzarotti et al., "Nanometer resolution imaging and tracking of fluorescent molecules with minimal photon fluxes," *Science*, vol. 355, no. 6325, pp. 606-612, 2017, doi: 10.1126/science.aak9913.
- [8] Y. Eilers, H. Ta, K. C. Gwosch, F. Balzarotti, and S. W. Hell, "MIN-FLUX monitors rapid molecular jumps with superior spatiotem-poral resolution," P. Natl. Acad. Sci USA, vol. 115, no. 24, pp. 6117-6122, 2018, doi: 10.1073/pnas.1801672115.
- [9] D. W. Pohl, W. Denk, and M. Lanz, "Optical stethoscopy: Image recording with resolution λ/20," *Appl. Phys. Lett.*, vol. 44, no. 7, pp. 651-653, 1984, doi: 10.1063/1.94865.
- [10] U. Dürig, D. W. Pohl, and F. Rohner, "Near-field optical-scanning microscopy," J. Appl. Phys., vol. 59, no. 10, pp. 3318-3327, 1986, doi: 10.1063/1.336848.
- [11] A. Harootunian, E. Betzig, M. Isaacson, and A. Lewis, "Superresolution fluorescence near-field scanning optical microscopy," Appl. Phys. Lett., vol. 49, no. 11, pp. 674-676, 1986, doi: 10.1063/1.97565.
- [12] M. G. L. Gustafsson, "Surpassing the lateral resolution limit by a factor of two using structured illumination microscopy," J. Microsc., vol. 198, no. 2, pp. 82-87, 2000, doi: 10.1046/j.1365-2818.2000.00710.x.
- [13] R. Heintzmann and M. G. L. Gustafsson, "Subdiffraction resolution in continuous samples," *Nat. Photon.*, vol. 3, no. 7, pp. 362-364, 2009, doi: 10.1038/nphoton.2009.102.
- [14] D. Li et al., "Extended-resolution structured illumination imaging of endocytic and cytoskeletal dynamics," *Science*, vol. 349, no. 6251, p. aab3500, 2015, doi: 10.1126/science.aab3500.
- [15] I. J. Cox and C. J. R. Sheppard, "Information capacity and resolution in an optical system," J. Opt. Soc. Am. A, vol. 3, no. 8, pp. 1152-1158, 1986, doi: 10.1364/JOSAA.3.001152.
- [16] A. B. Samokhin and A. S. Samokhina, "3D Fredholm integral equations for scattering by dielectric structures," *Diff. Equat.*, vol. 52, no. 9, pp. 1178-1187, 2016, doi: 10.1134/S0012266116090093.
- [17] R. W. Gerchberg, "A practical algorithm for the determination of phase from image and diffraction plane pictures," *Optik*, vol. 35, pp. 237-246, 1972.
- [18] Y. Shechtman, Y. C. Eldar, O. Cohen, H. N. Chapman, J. Miao, and M. Segev, "Phase Retrieval with Application to Optical Imaging: A contemporary overview," *IEEE Singal Proc. Mag.*, vol. 32, no. 3, pp. 87-109, 2015, doi: 10.1109/MSP.2014.2352673.
- [19] G. Barbastathis, A. Ozcan, and G. Situ, "On the use of deep learning for computational imaging," *Optica*, vol. 6, no. 8, pp. 921-943, 2019, doi: 10.1364/OPTICA.6.000921.
- [20] A. Sinha, J. Lee, S. Li, and G. Barbastathis, "Lensless computational imaging through deep learning," *Optica*, vol. 4, no. 9, pp. 1117-1125, 2017, doi: 10.1364/OPTICA.4.001117.
- [21] Y. Rivenson, Y. Zhang, H. Günaydın, D. Teng, and A. Ozcan, "Phase recovery and holographic image reconstruction using deep learning in neural networks," *Light: Sci. Appl.*, vol. 7, no. 2, pp. 17141-17141, 2018, doi: 10.1038/lsa.2017.141.
- [22] A. Szameit et al., "Sparsity-based single-shot subwavelength coherent diffractive imaging," *Nat. Mater.*, vol. 11, no. 5, pp. 455-459, 2012, doi: 10.1038/nmat3289.
- [23] S. Gazit, A. Szameit, Y. C. Eldar, and M. Segev, "Super-resolution and reconstruction of sparse sub-wavelength images," *Opt. Ex*press, vol. 17, no. 26, pp. 23920-23946, 2009, doi: 10.1364/OE.17.023920.
- [24] E. Narimanov, "Resolution limit of label-free far-field microscopy," Adv. Photon., vol. 1, no. 5, p. 056003, 2019. doi: 10.1117/1.AP.1.5.056003.

- [25] V. Vemuri and G.-S. Jang, "Inversion of Fredholm integral equations of the first kind with fully connected neural networks," J. Frankl. Inst., vol. 329, no. 2, pp. 241-257, 1992, doi: 10.1016/0016-0032(92)90031-B.
- [26] M. V. Berry and S. Popescu, "Evolution of quantum superoscillations and optical superresolution without evanescent waves," J. Phys. A: Math. Gen., vol. 39, no. 22, p. 6965, 2006, doi: 10.1088/0305-4470/39/22/011.
- [27] F. M. Huang, N. Zheludev, Y. Chen, and F. J. G. d. Abajo, "Focusing of light by a nanohole array," *Appl. Phys. Lett.*, vol. 90, no. 9, 2007, doi: 10.1063/1.2710775.
- [28] M. V. Berry, "Quantum backflow, negative kinetic energy, and optical retro-propagation," J. Phys. A: Math. Theor., vol. 43, p. 415302, 2010 doi: 10.1088/1751-8113/43/41/415302.
- [29] G. Yuan, E. T. F. Rogers, and N. I. Zheludev, ""Plasmonics" in free space: observation of giant wavevectors, vortices, and energy backflow in superoscillatory optical fields," *Light: Sci. Appl.*, vol. 8, no. 2, 2019, doi: 10.1038/s41377-018-0112-z.
- [30] J. F. Nye, M. V. Berry, and M. E. R. Walford, "Measuring the change in thickness of the Antarctic ice sheet," *Nature*, vol. 240, no. 97, pp. 7-9, 1972.
- [31] J. F. Nye and M. V. Berry, "Dislocations in wave trains," P. Roy. Soc. A, vol. 336, pp. 165-90, 1974.
- [32] T. Pu, J.-Y. Ou, V. Savinov, G. Yuan, N. Papasimakis, and N. I. Zheludev, "Unlabeled Far-Field Deeply Subwavelength Topological Microscopy (DSTM)," Adv. Sci., vol. 8, no. 1, p. 2002886, 2020, doi: 10.1002/advs.202002886.
- [33] T. Pu, J. Y. Ou, N. Papasimakis, and N. I. Zheludev, "Label-free deeply subwavelength optical microscopy," *Appl. Phys. Lett.*, vol. 116, p. 131105, 2020 doi: 10.1063/5.0003330.
- [34] C. Rendón-Barraza, E. A. Chan, G. Yuan, G. Adamo, T. Pu, and N. I. Zheludev, "Deeply sub-wavelength non-contact optical metrology of sub-wavelength objects," APL Photon., vol. 6, no. 6, p. 066107, 2021, doi: 10.1063/5.0048139
- [35] T. Liu et al., "Picophotonic localization metrology beyond thermal fluctuations," *Nat. Mater.*, pp. 844–847, 2023, doi: 10.1038/s41563-023-01543-y.
- [36] C. H. Chi, E. Plum, N. I. Zheludev, and K. F. MacDonald, "Robust Optical Picometrology Through Data Diversity," Opt. Mater. Express, 2024.
- [37] J. W. Goodman, Introduction to Fourier Optics. Roberts and Company Publishers, 2005.
- [38] G. Yuan and N. I. Zheludev, "Optical superoscillation technologies beyond the diffraction limit," Nat. Rev. Phys., vol. 4, pp. 16-32, 2022. doi: 10.1038/s42254-021-00382-7.
- [39] G. Yuan, K. S. Rogers, E. T. F. Rogers, and N. I. Zhelludev, "Far-field superoscillatory metamaterial superlens," *Phys. Rev. Appl.*, vol. 11, no. 6, p. 064016, 2019, doi: 10.1103/PhysRevApplied.11.064016.
- [40] N. I. Zheludev, "What diffraction limit?," Nat. Mater., vol. 7, pp. 420-422, 2008, doi: 10.1038/nmat2163

- [41] F. M. Huang and N. I. Zheludev, "Super-resolution without evanescent waves," *Nano Lett.*, vol. 9, no. 3, pp. 1249-54, p. 091119, 2009, doi: 10.1021/nl9002014.
- [42] G. Yuan and N. I. Zheludev, "Detecting nanometric displacements with optical ruler metrology," *Science*, vol. 364, no. 6442, pp. 771-775, 2019, doi: 10.1126/science.aaw7840.
- [43] S. Kay, Fundamentals of Statistical Processing: Estimation Theory. 1993.
- [44] J. Chao, E. Sally Ward, and R. J. Ober, "Fisher information theory for parameter estimation in single molecule microscopy: tutorial," J. Opt. Soc. Am. A, vol. 33, no. 7, pp. B36-B57, 2016 doi: 10.1364/JOSAA.33.000B36.
- [45] Y. Shechtman, S. J. Sahl, A. S. Backer, and W. E. Moerner, "Optimal Point Spread Function Design for 3D Imaging," *Phys. Rev. Lett.*, vol. 113, no.13, p. 133902, 2014 doi: 10.1103/PhysRevLett.113.133902.
- [46] M. Tsang, R. Nair, and X.-M. Lu, "Quantum Theory of Superresolution for Two Incoherent Optical Point Sources," *Phys. Rev. X*, vol. 6, no. 3, p. 031033, 2016, doi: 10.1103/PhysRevX.6.031033.
- [47] M. Tsang, H. M. Wiseman, and C. M. Caves, "Fundamental Quantum Limit to Waveform Estimation," *Phys. Rev. Lett.*, vol. 106, no. 9, p. 090401, 2011, doi: 10.1103/PhysRevLett.106.090401.
- [48] F. Yang, R. Nair, M. Tsang, C. Simon, and A. I. Lvovsky, "Fisher information for far-field linear optical superresolution via homodyne or heterodyne detection in a higher-order local oscillator mode," *Phys. Rev. A*, vol. 96, no. 6, p. 063829, 2017, doi: 10.1103/PhysRevA.96.063829.
- [49] V. Giovannetti, S. Lloyd, and L. Maccone, "Advances in quantum metrology," Nat. Photon., vol. 5, no. 4, pp. 222-229, 2011, doi: 10.1038/nphoton.2011.35.
- [50] J. Hüpfl et al., "Continuity equation for the flow of Fisher information in wave scattering," *Nat. Phys.*, vol. 20, no. 8, pp. 1294-1299, 2024, doi: 10.1038/s41567-024-02519-8.
- [51] M. Horodynski, D. Bouchet, M. Kühmayer, and S. Rotter, "Invariance Property of the Fisher Information in Scattering Media," Phys. Rev. Lett., vol. 127, no. 23, p. 233201, 2021, doi: 10.1103/PhysRevLett.127.233201.
- [52] D. Bouchet, L. M. Rachbauer, S. Rotter, A. P. Mosk, and E. Bossy, "Optimal Control of Coherent Light Scattering for Binary Decision Problems," *Phys. Rev. Lett.*, vol. 127, no. 25, p. 253902, 2021, doi: 10.1103/PhysRevLett.127.253902.
- [53] D. Bouchet, S. Rotter, and A. P. Mosk, "Maximum information states for coherent scattering measurements," *Nat. Phys.*, vol. 17, no. 5, pp. 564-568, 2021, doi: 10.1038/s41567-020-01137-4.
- [54] D. Bouchet and E. Bossy, "Temporal shaping of wave fields for optimally precise measurements in scattering environments," *Phys. Rev. Res.*, vol. 5, no. 1, p. 013144, 2023, doi: 10.1103/PhysRevResearch.5.013144.